Journal Pre-proof

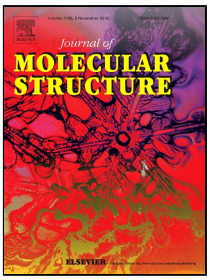

Structural, vibrational, optical properties and theoretical studies of a new organic-inorganic material: Tris-acetoguanaminium hexachlorobismuthate monohydrate

Saida Ben Ali, Valeria Ferretti, Lucia Del Bianco, Federico Spizzo, Mohamed Belhouchet

PII:	S0022-2860(19)31083-X
DOI:	https://doi.org/10.1016/j.molstruc.2019.126986
Article Number:	126986
Reference:	MOLSTR 126986
To appear in:	*Journal of Molecular Structure*
Received Date:	01 June 2019
Accepted Date:	25 August 2019

Please cite this article as: Saida Ben Ali, Valeria Ferretti, Lucia Del Bianco, Federico Spizzo, Mohamed Belhouchet, Structural, vibrational, optical properties and theoretical studies of a new organic-inorganic material: Tris-acetoguanaminium hexachlorobismuthate monohydrate, *Journal of Molecular Structure* (2019), https://doi.org/10.1016/j.molstruc.2019.126986

Structural, vibrational, optical properties and theoretical studies of a new organic-inorganic material: Tris-acetoguanaminium hexachlorobismuthate monohydrate

Saida Ben Ali[a], Valeria Ferretti[b], Lucia Del Bianco[c], Federico Spizzo[c], Mohamed Belhouchet[a]

[a] Laboratory Physico-Chemistry of the Solid State, Department of Chemistry, Faculty of Sciences of Sfax, B. P. 1171, 3000, Sfax, Tunisia

[b] Department of Chemical and Pharmaceutical Sciences, Centre for Structural Diffractometry, University of Ferrara, Via L. Borsari 46, I-44121 Ferrara, Italy.

[c] Department of Physics and Earth Sciences, University of Ferrara, Via G. Saragat 1, I-44122 Ferrara Italy.

Corresponding Author: belhouchet2002@yahoo.fr

Abstract

In the present work, we investigate a self-assembly process which offers the possibility to construct organic-inorganic hybrid architectures by assembling halogenobismuthates(III) as building units and organic cations, in order to elaborate a new organic inorganic hybrid material with the formula $\{[H\text{-}guan]_3[BiCl_6].H_2O\}$ ($H\text{-}guan^+$: acetoguanaminium cation). The compound was synthesized by slow evaporation of aqueous solution at room temperature and characterized by X-ray single crystal diffraction, infrared and UV-vis absorption, scanning calorimetry (DSC) and thermogravimetric analysis (TGA). Its structure consists of $[BiCl_6]^{3-}$ anions, showing distorted octahedral geometry, surrounded by three crystallographically independent acetoguanaminium $[C_4H_8N_5]^+$ cations and a water molecule. The crystal packing is governed by the formation of a number of N–H…Cl, N–H…N, N–H…O and O–H…Cl hydrogen bonds arranged in a three-dimensional network. The optical properties of the title compound were also investigated by both UV–vis and photoluminescence spectroscopy. DFT calculations at the B3LYP/LanL2DZ level have been carried out to gain a better insight into its vibrational and optical properties and a good agreement was found between experiments and calculations. TGA coupled to DSC analysis were carried out to study the thermal behavior of the prepared material.

Key words: Hybrid material, Hexachlorobismuthate, X-ray diffraction, DFT calculations

1. Introduction

Currently, the synthesis of organic–inorganic hybrid materials based on metal halide units has taken a great attention due to their interesting structural diversity [1-5]. They are considered potential platforms for various new applications in extremely diverse fields due to their peculiar physico-chemical features such as nonlinear optical activity and electronic properties [6-9]. As for the metal-halide systems, significant efforts have been made to combine halogenobismuthates compounds with aromatic cations, in order to explore the wealthy diversity in their structural and physical properties, especially their potential semiconducting behavior. Thus, several studies were carried out in solid state on complexes of bismuth (III), in particular complexes of bismuth (III) chlorides, with molecular organic components.

The bismuth coordination geometry appears to be influenced by the nature of the halogen atom and by the cation size and charge, but the most important factor seems to be the number of the hydrogen bond donor sites of the organic template [10-11]. As already pointed out in several works, the anionic sub lattices are built of MX_6^{3-} distorted octahedra which can be connected via corners, edges or faces sharing, in such a way that three halogen atoms of the Bi coordination sphere are bridging and three are terminal; this can lead to the formation of isolated molecules (0D), infinites chains (1D) two (2D) or three (3D) dimensional networks [12-15]. Great effort has been placed on determining the crystal structures of this kind of materials, while spectroscopic and optical studies are relatively less studied.

The present work focuses on the synthesis of a new organic-inorganic compound containing hexachloro-bismuthate (III) and the commercial 2,4-diamino-6-methyl-1,3,5-triazine, $[H\text{-guan}]_3[BiCl_6].H_2O$ (guan=Acetoguanamine). Besides the chemical synthesis, we report its structural characterization by single crystal X-ray diffraction, Fourier transform infrared (FT-IR) and optical measurement by photoluminescence and absorption. The TD/DFT (B3LYP/LanL2DZ) approach was used for the interpretation of the experimental vibrational and optical absorption spectra, and to calculate the Mulliken atomic charges. Electronic properties such as HOMO and LUMO energies were determined. Differential scanning calorimetry (DSC) and the thermogravimetric analysis (TGA) were also implemented to study the thermal behavior of the title compound.

2. Experimental

2. 1. Synthesis

Bismuth (III) nitrate pentahydrate and acetoguanamine {6-methyl-1,3,5-triazine-2,4-diamine} were dissolved in a concentrated HCl solution in the presence of distilled water and

ethanol in a stoichiometric ratio. The obtained solution was well stirred and kept to evaporate at room temperature. After several days of slow evaporation, we obtained colourless single crystals of $[H\text{-guan}]_3[BiCl_6].H_2O$ (yield: 80%).

2. 2. X-Ray data collection

Single crystal sized (0.30, 0.29, 0.09) mm^3 was carefully selected to perform its structural analysis by X-ray diffraction. The crystallographic data were collected on a Nonius Kappa CCD diffractometer at room temperature using graphite-monochromated MoKα radiation (λ= 0.71073 Å) with a φ scan followed by ω scan to fill the sphere. All intensities were corrected for Lorentz, polarization and absorption effects [16]. The structure was solved by direct methods with the SIR97 program [17] and refined on F^2 by full-matrix least-squares methods with anisotropic non-H atoms. The H atoms were included on calculated positions, riding on their carrier atoms, while the remaining hydrogens were found in the difference Fourier map and refined isotropically. Hydrogen atoms of water molecule were refined with restrained distances (O-H = 0.86(2) Å). All other calculations were accomplished using SHELX97 [18] and WingX [19]. Crystal data are given in Table 1. The graphical representations were made with ORTEP [20] and Diamond [21] programs.

2.3. Physicochemical characterization techniques

The infrared absorption spectrum was recorded at room temperature on a JASCOFT-IR-420 spectrometer using a crystal sample in the range 400-4000 cm^{-1}.

Photoluminescence spectrum was recorded at room temperature on a Perkin-Elmer LS55 fluorescence spectrometer processed with a 350 nm radiation as the excitation source. The optical absorption spectrum of the films was recorded at room temperature using a UV–Vis absorption spectrophotometer (Hitachi, U-3300) in the wavelength range of 200-800 nm.

Simultaneous differential scanning calorimetry and thermogravimetry analyses were carried out using a NETZSCH TASC 409. The sample, in form of powder (~ 11 mg), was put in an alumina crucible, and the measurements were performed in nitrogen atmosphere in the 30 ^oC – 800 ^oC temperature range with a 5 ^oC/min heating rate.

2.4. Theoretical calculations details

The vibrational frequencies calculations and molecular geometry optimization of the title material were supported by DFT method using the Lee–Yang–Parr correlation functional (B3LYP) with the LanL2DZ basis set [22, 23] implemented within Gaussian 03 program [24]. All the parameters were allowed to relax and all the calculations converged to an optimized geometry which corresponds to an energy minimum as revealed by the lack of imaginary values in the calculated wavenumbers. The calculated vibrational wavenumbers were scaled

and compared with the experimental spectra. For visual comparison, we have superposed experimental and simulated IR spectra. The chemical reactivity descriptor from Mulliken population method has also been investigated.

3. Results and discussion

3.1. Crystal structure

The organic–inorganic compound formulation, $[H\text{-guan}]_3[BiCl_6].H_2O$, was unequivocally determined by X-ray diffraction analysis.

As shown in Fig.1, the asymmetric unit is constituted by one hexachlorobismuthate $[BiCl_6]^{3-}$ anion, three protonated $[H\text{-guan}]^+$ cations and a water molecule. The bismuth (III) atom is bounded to six chlorine atoms; the coordination geometry is distorted octahedral, as it can be deduced from the value of both the Bi–Cl bond lengths, ranging from 2.5709(15) to 2.8602(4) Å, and the Cl–Bi–Cl angles, ranging from 86.65(5)° to 95.78 (6)° for cis arrangements and from 173.79(5)° to 176.06(5)° for trans arrangements (Table 2). The structural parameters of the present compound agree well with those found in similar compounds characterized by $[BiCl_6]^{3-}$ octahedral units [25-29]. The calculated average values of the Baur distortion indices [30] corresponding to the different angles and distances in the $[BiCl_6]^{3-}$ entities are ID (Bi–Cl)=0.0067 and ID(Cl–Bi–Cl)=0.000052. The Baur's distortion values show that the coordination geometry of the Bi(III) metal is slightly distorted. In fact, this distortion is correlated firstly to the deformation resulting from the stereochemical activity of Bi lone electron pair, and secondly to the deformation caused by the interactions between $[BiCl_6]^{3-}$ octahedron and neighbors molecules through different hydrogen bonds [31]. In the crystal, the involvement of any chlorine atom in hydrogen bonding results in a shift of the lone electron pair of the Bi atom in the direction of the H atom, which generally leads to an increase of the Bi-Cl distance. In the present structure, such a behavior is observed for Bi-Cl5, Bi-Cl6, Bi-Cl2 and Bi-Cl1 bond lengths which are longer than the others.

The three chemically identical monoprotonated cations $[H\text{-guan}]^+$ are crystallographically independent and are noted respectively: H-guan (1) {N1, N2, N3}, H-guan (2) {N6, N7, N8} and H-guan (3) {N11, N12, N13}. The values of the internal C2-N2-C1, C6-N7-C5 and C10-N13-C11 angles (Table 3) of 120.2(5), 119.9(5) and 120.1(4)°, respectively, are larger than the other C-N-C angles found in the triazine ring of neutral 2,4-diamino-6-methyl-1,3,5-triazine (acetoguanamine); this fact is a further indication of the nitrogen protonation [7-8], besides the localization in the difference Fourier map of the hydrogen bond to N2, N7 and N13 atoms.

The overall structural arrangement of the title hybrid material is shown in Fig. 2. It can be described as an alternation of organic-inorganic layers parallel to (011) plane. The inorganic framework is constituted by $[BiCl_6]^{3-}$ anions and water molecules. Pairs of water molecule are linked to two neighboring $[BiCl_6]^{3-}$ anion by means of centrosymmetric O-H…Cl interactions (O1W-H...Cl6^{vi} and O1W-H...Cl5) to form isolated dimers with the formula $[(BiCl_6)_2(H_2O)_2]^{6-}$ (Fig. 3 (a) and (b)).

In the organic layers the three acetoguanaminium cations interact with the neighbor cations through a pair of weak N-H…N hydrogen bonds between the amine groups (as donors) and the non protonated ring N atoms (as acceptors), to form a one dimensional organic cations trimers, denoted $\{H\text{-}guan^+\}_3$, running along the a-axis. These trimers are connected through a pair of centrosymmetric hydrogen bond interactions (N9-H9A…N6^{i}) between the neighboring $\{H\text{-}guan^+\}_3$, forming a six-membered ribbon denoted $\{H\text{-}guan^+\}_6$ with $R_2^2(8)$ ring motif (Fig. 4 and table 4). Therefore, these cationic ribbons are inter-linked by the anionic dimers which, as multiple acceptors, interact in turn with one donor acetoguanaminium through the protonated N atom (N2-H2…Cl5, N13-H13…Cl2^{iv}), and multiple donor amine groups (N4-H4B…Cl3, N5-H5A...Cl6^{ii}, N9-H9…Cl1, N10-H10…Cl1^{i}, N13—H13…Cl2^{iv}, N14-H14A…Cl5^{v}, N14-H14B…Cl2iv, N15-H15B…Cl4^{vi}) (Fig. 4). Indeed, the octahedral $[BiCl_6]^{3-}$ complex acts as a multiple H-bond acceptor whose donor-acceptor distances are in the range 3.137(4) - 3.553 (6) Å (Table 4). Also, the N7-H group in $[H\text{-}guan]^+$(2) cation acts as hydrogen bonding donor towards the cocrystallized water molecule.

Moreover, the analysis of inter-centroid distances between two neighboring $[H\text{-}guan]^+$ cations shows that only $[H\text{-}guan]^+$ (3) cations are involved in π…π interactions, since the maximum distance accepted for this type of interaction is equal to 3.80 Å [32] (Fig.5 and Table 4).

3.2. FT-IR spectral analysis

To get more information on the structure of the title compound, we have carried out a vibrational study using infrared spectroscopy at room temperature and compared the experimental spectrum with the calculated one, as shown in Fig.6. To identify clearly the characteristic vibrational modes of this organic-inorganic system, we leaned on analogies with other previously reported vibrational studies of similar materials. The detailed assignments of experimental and calculated bands of the title compound are listed in Table 5.

As shown in Fig. 6, the DFT calculations indicate that the inorganic entities lead to vibrations below 400 cm^{-1} which are not observed experimentally in our conditions. The

calculated spectrum expected the (Bi-Cl) symmetric and asymmetric stretching at 166 and 290 cm^{-1}. Thus, according to the previous works on $[Bi\text{-}Cl_6]^{3-}$ anions, the internal vibrational modes of Bi-Cl appear below 400 cm^{-1} [33-34]. That way, we focused only on the vibration modes of the $[H\text{-}guan]^{+}$ cation. The high frequencies domain is characterized by (N-H) and (C-H) stretching modes. Thus, the asymmetric and symmetric N-H stretching vibrations in the organic cation are observed at higher frequency. In fact, as seen in the IR spectrum, the medium peaks observed between 3303 cm^{-1} and 3189 cm^{-1} are assigned to the stretching asymmetric and symmetric vibrations of the (N-H) bands. According to DFT calculations, the signals of these modes appear between 3092 cm^{-1} and 3428 cm^{-1}, in agreement with what observed in similar compounds [12, 35]. The stretching modes $\nu_s(CH_3)$ and $\nu_{as}(CH_3)$ are observed between 3059 cm^{-1} and 2852 cm^{-1}. Also, the band observed at 2621cm^{-1} is assigned to the combination bands and overtones ($\nu_{calculated}$=2435 cm^{-1}) [36].

In the studied compound, the scissoring asymmetric vibration $\delta_{as}(NH_2)$ has been identified experimentally as a very strong band at 1670 cm^{-1} [14]. It is identified by DFT calculations at 1690 cm^{-1} while the band located experimentally at 1624 cm^{-1} and predicted theoretically at 1640 cm^{-1} is assigned to scissoring symmetric vibration $\delta_s(NH_2)$. We noted strong peaks located experimentally at 1525, 1502 and 1490 cm^{-1} corresponding to $\omega(NH_2)$, $\delta_{as}(CH_3)$ and $\delta_s(CH_3)$ respectively. They are identified by DFT calculations at 1570, 1519 and 1492 cm^{-1}. Additionally, the stretching vibrations of the (C=N) band of the aromatic ring is observed at 1459 cm^{-1} [37]. The DFT calculations give this mode at 1449 cm^{-1}. Also, in this study, a medium band at 1269 cm^{-1} corresponding to $\omega(CH_3)$ was observed. The medium band located at 1174 cm^{-1} is assigned to the twisting vibration of the NH_2 group while the calculated wavenumber is detected at 1180 cm^{-1} [38-40]. Furthermore, the bands appearing between 1041-1089 cm^{-1} are attributed to ν_{as}(C-N-C) and ν_{as}(N-C-N. The calculated wavenumbers are given between1088 and 1094 cm^{-1}. The weak band detected at 1027cm^{-1} is attributed to the rocking of NH_2. The absorption bands observed at 1000 and 971cm^{-1} in the FT-IR spectrum are assigned to respectively to N-H in plane and out of plane bending. The strong peak at 786 cm^{-1} corresponds to the roking of the water molecule $\rho(H_2O)$ [41-42]. Besides, strong and medium bands observed between 627 cm^{-1} and 556cm^{-1} are assigned to the deformation modes δ(C-N-C), δ(C-C-N) and (N-C-N). Even if there are some differences, the experimental and calculated IR spectra of the studied compound are similar allowing a good correlation between experimental and theoretical data (Fig. 7). Thus, the precision is well sufficient to assign the experimental frequencies and to confirm the attribution proposed above.

3.3. Optical properties

3.3.1. Absorption and photoluminescence

The experimental UV–vis absorption (Abs) and Photoluminescence (PL) spectra of the title compound, measured at room temperature, are illustrated in Fig. 8. According to various studies reported on the halogenobismuthates (III), the absorption spectrum exhibits several bands between 300 and 400 nm [26, 43-44]. Some suggestions in the literature assigned these bands mostly to Metal-Centred (MC) transitions [38]. However, recent studies have proved that some of these bands, particularly those of higher energies, can be attributed partially to the Ligand to metal charge transfer (LMCT) transition. Furthermore, in chlorobismuthate hybrid materials containing $[BiCl_6]^{3-}$anions, the highest occupied molecular orbital (HOMO) is predominately $6s^2$ and the lowest unoccupied molecular orbital (LUMO) is predominately 6p [43, 45].

The absorption spectrum of the title compound exhibits four absorption bands centered at 218 nm, 264 nm, 332 nm and 441 nm. The two first bands at 218 and 264 nm corresponding to the higher energies bands 5.68 eV and 4.69 eV respectively, are assigned to the (LMCT) transition from the np orbital of Cl to 6p orbital of Bi(III) since the (LMCT) transitions from chlorine to Bi(III) are expected to occur at relatively high energies. The third band at 332 nm (3.73eV) is attributed to the 6s6p MC transition from the $6s^2$ to the T_{1u} state which correlates with the $^3P1$ atomic state in Bi(III). Nevertheless, the weak band at 441 nm (2.81 eV) may be assigned to the π–π* electronic transition within the acetoguanaminium rings [46-47].

The luminescence spectrum is recorded under the excitation of 375 nm at room temperature. As shown in Fig .8, this compound exhibits one luminescence peak at 520 nm (2.38eV). This material manifests blue luminescence in the solid state. We attribute this emission band to the electronic transitions within the chlorobismuthate inorganic part. The luminescence properties are comparable with those found for other BiCl-based hybrid materials [48-50]. The combination of a narrow emission line width and a blue color proved that the studied compound can be used in high-performance LED applications [51-54].

3.3.2. HOMO–LUMO analysis

TD-DFT/B3LYP/LanL2DZ calculations were performed with the aim to study in detail the optical behavior of this new synthesized material and to better understand its electronic structure. As seen in Fig. 9, there are four distinct absorption peaks at 218, 264, 332 and 441 nm whereas the theoretical calculation predicts clearly only one intense electronic transition at 320 nm (3.87 eV). The calculated band, corresponding to an electronic transition from the highest occupied molecular orbital (HOMO) to the lowest un-occupied molecular orbital

(LUMO), agrees well with the optical absorption band observed in the UV-Vis absorption spectrum of thin films at 332 nm (3.73 eV). The shift between experimental and calculated transition energies is found to be around 0.14 eV and is commonly observed in TD-DFT calculations using the B3LYP functional [15, 55-56]. Surfaces representing the HOMO and LUMO frontier orbitals, calculated at the B3LYP/LanL2DZ level, are shown in Fig. 10. It is worth noting that the energy values of these orbitals and the energy gap between them are strictly related to both the optical and the electrical transport properties. The energy separation between the HOMO and LUMO (i.e. the band gap) is of 3.71 eV (Fig. 10), which corresponds to the band observed at 3.73 eV. According to isodensity plots, the HOMO electrons are localized on the inorganic part of the crystal and are principally composed of Bi and Cl atoms orbitals, while LUMO is almost mainly organic in character. This means that the electronic transition occurs from the [H-guan]$^{+}$ cation to $[BiCl_6]^{3-}$ anion and highlights the importance of intra-molecular charge transfer from electron-donor groups to electron-acceptor groups via conjugated path. Gauss-Sum 2.2 program [57] was used to prepare the density of state (DOS) and calculate group contributions to the molecular orbitals (HOMO and LUMO) as shown in Fig. 11. DOS plot shows population analysis per orbital and demonstrates a simple view of the character of the molecular orbitals in a certain energy range.

3.4. Mulliken Atomic Charges

Mulliken charge analysis is directly related to the method of vibrational analysis of the molecule and is also used to quantify how the electronic structure changes under atomic displacement. Atomic charges were obtained from ab-initio molecular orbital calculation using B3LYP level with LanL2DZ basis set. The Mulliken charge distribution structure of $[H\text{-}guan]_3BiCl_6.H_2O$ is shown in Fig. 12. The H atoms bound to N or O atoms (NH, NH_2 or H_2O groups) have bigger and more positive charges than the other hydrogen atoms. All hydrogen atoms are positively charged. This obtained result proves the effect of their binding to electronegative nitrogen and oxygen atoms. Thus, oxygen atoms have negative charge. It is important to mention that the intermolecular hydrogen bonds created in this compound have confirmed these results. The charge distribution of the material shows that C4, C8 and C12 of [H-guan]$^{+}$ exhibit a negative charge because they are attached to electropositive hydrogen atoms of methyl group and carbon atoms of the rings whereas the other carbon atoms, which are linked to electronegative nitrogen atoms of NH_2 and NH groups, exhibit positive charges. We can remark that the carbon atom is highly influenced by their substitutes [58-59]. Moreover, the charge distribution shows that the chlorine and oxygen atoms have strong negative charges because they are involved, as acceptor, in hydrogen bonds. It's very

important to note that the maximum atomic charge is noticed on the bismuth atom when compared with other atoms because it is surrounded by six electronegative chloride atoms [60].

3.6. Thermal analysis

The thermal stability of the title compound was investigated performing simultaneous DSC/TGA thermal analyses in the 30 °C – 800 °C temperature range in nitrogen purge gas with a 5°C/min average heating rate. The analysis results illustrated in Fig.13 reveal that the synthesized compound is thermally stable up to 160 °C. Upon heating , the crystal undergoes a dehydration peak at 174°C, starting at 164 °C and ending at 195 °C, (observed weight loss, 2.63%; calculated weight loss, 2.2%), attributed to the elimination of the water molecule. After dehydration, the DSC curve shows three endothermic peaks, the first peak at 214 °C, the second one at 282 °C which is more intense and the third at 355 °C (Fig.13). These peaks can be attributed to the decomposition of the organic part of the anhydrous compound in a wide temperature range (197 °C- 380 °C). The decomposition of the three cations is confirmed by 47.2 % weight loss observed in the TGA curve, which is close to the calculated value of 46% [61-62]. Besides, the weight loss observed in the temperature range from 400 to 625 °C corresponds to the release of the rest of the compound, in particular volatile substances such as Cl_2 molecules [25]. The fact that the final residue is very small is also confirmed by the weighing of the mass of the solid residue that we removed from the alumina crucible after performing the treatment. In conclusion, the thermal study of the hybrid bismuth compound suggests that crystal can be used for some applications such as optoelectronic devices at temperatures lower than 160 °C.

4. Conclusion

In summary, this work describes the chemical preparations, vibrational, optical properties, thermal analysis and structural determination of a new $[H\text{-guan}]_3[BiCl_6].H_2O$ compound. Its single-crystal X-Ray crystallographic structure shows that four types of hydrogen bonds; N-H···Cl, N-H···O, N-H···N and O-H···Cl contribute to the cohesion and stability of the crystalline lattice. Also, the molecular structure of the studied compound is stabilized by π–π interactions. Infrared spectroscopy made it possible to determine the assignments of the observed frequencies to the various modes of vibration. The vibrational spectrum calculated at the DFT/B3LYP/LanL2DZ level of theory shows good agreement with experimental results. The optical properties of this compound were investigated by absorption measurements which show four distinct absorption bands centered at 218 nm, 264 nm, 332 nm and 441 nm and a strong blue luminescence emission at 520 nm (2.38 eV). HOMO-

LUMO energy gap and DOS have been calculated using quantum chemical computations to explore possible charge transfer processes that take place inside the molecule. The thermal study (TGA and DSC) confirms the stability of this compound.

Supplementary materials

CCDC 1907441 contains supplementary crystallographic data for the current compound. This data can be obtained free of charge via http:// www.ccdc.cam.ac.uk/conts/retrieving.html, or from the Cambridge Crystallographic Data center, 12 Union Rood, Cambridge CB2 1EZ, UK (Fax: (international) +44 1223/336 033; e-mail: deposit@ccdc.cam.ac.uk).

Acknowledgements

The authors would like to thank Mr. N. ELGHOUL from Agareb School for his help with English.

References

[1] J. Calabrese, N.L. Jones, R.L. Harlow, N. Herron, D.L. Thorn, Y. Wang, J. Am. Chem. Soc. 113 (1991) 2328.

[2] G. C. Papavassiliou, Prog. J. Solid St. Chem. 25 (1997) 125.

[3] M. Wojtas, R. Jakubas. J. Phys. Condens. Matter 16 (2004) 7521.

[4] J. Zhai, R. L. Sang, L. Xu, J. Mol. Struct. 1006 (2011) 553.

[5] R. Jakubas, L. Sobczyk, Phase Transitions 20 (1990) 163.

[6] M. Wojtas, R. Jakubas, Z. Ciunik, W. Medycki, J. Solid State Chem. 177 (2004) 1575.

[7] M. Bujak, R. J. Angel, J. Solid State Chem. 178 (2005) 2237.

[8] L. M. Wu, X. T. Wu, L. Chen, Coord. Chem. Rev. 253 (2009) 2787.

[9] S. Chaabouni, A. Hadrich, F. Romain, A. Ben Salah, J. Solid State Sci. 5 (2003) 1041.

[10] B. Kulicka, T. Lis, V. Kinzhybalo, R. Jakubas, A. Piecha, Polyhedron 29 (2010) 2014.

[11] H. Dammak, S. Triki, A. Mlayah, Y. Abid, H. Feki, J. Lumin. 166 (2015) 180.

[12] H. Khili, N. Chaari, A. Madani, N. Ratel-Ramond, J. Jaud, S. Chaabouni, Polyhedron 48 (2012) 146.

[13] Z. Aloui, V. Ferretti, S. Abid, M. Rzaigui, F. Lefebvre, C. Ben Nasr, J. Mol. Struct. 1087 (2015) 26.

[14] Z. Aloui, V. Ferretti, S. Abid, F. Lefebvre, M. Rzaigui, C. Ben Nasr, J. Mol. Struct. 1097 (2015) 166.

[15] H. Dammak, H. Feki, H. Boughzela, Y. Abid, Spectrochim. Acta A 137 (2015) 1235.

[16] R.H. Blessing, Acta Crystallogr. A51(1995) 33.

[17] A. Altomare, M. C. Burla, M. Camalli, G. Cascarano, C. Giacovazzo, A. Guagliardi, A. A. G. Moliterni, G. Polidori, R. Spagna, J. Appl. Cryst. 32, (1999) 115.

[18] G.M. Sheldrick, SHELXL-97: Program for Crystal Structure Refinement; University of Göttingen: Göttingen, Germany, 1997

[19] L. J. Farrugia, J. Appl. Crystallogr. 32 (1999) 837

[20] L. J. Farrugia, J. Appl Cryst. 30 (1997) 565.

[21] K. Brandenburg, Diamond Version 2.0 Impact GbR, Bonn, Germany, 1998.

[22] N. Zhanpelsov, M. Matsuoka, H. Yamashite, M. Anpo, J. Phys. Chem. B. 102 (1998) 6915.

[23] N. Niclasc, M. Dolg, H. Stoll, H. Preuss, J. Phys. Chem. 102 (1995) 8942.

[24] M.J. Frisch, G.W. Trucks, H.B. Schlegel, G.E. Scuseria, M.A. Robb, J.R. Cheeseman, V.G. Zakrzewski, J.A. Montgomery Jr., R.E. Stratmann, J.C. Burant, S. Dapprich, J.M. Millam, A.D. Daniels, K.N. Kudin, M.C. Strain, O. Farkas, J. Tomasi, V. Barone,M. Cossi, R. Cammi, B. Mennucci, C. Pomelli, C. Adamo, S. Clifford, J. Ochterski,G.A. Petersson, P.Y. Ayala, Q. Cui, K. Morokuma, D.K. Malick, A.D. Rabuck, K.Raghavachari, B. Foresman, J. Cioslowski, J.V. Ortiz, A.G. Baboul, B.B. Stefanov,G. Liu, A. Liashenko, P. Piskorz, I. Komaromi, R. Gomperts, R.L. Martin, D.J. Fox,T. Keith, M.A. Al-Laham, C.Y. Peng, A. Nanayakkara, M. Challacombe, P.M.W.Gill, B. Johnson, W. Chen, M.W. Wong, J.L. Andres, C. Gonzalez, M. Head-Gordon, E.S. Replogle, J.A. Pople, Gaussian 03, Revision C. 02, Gaussian, Inc,Wallingford, CT, 2004.

[25] Z. Ouerghi, H. Gornitzka, E. Temel, I. Dridi, R. Kefi, J. Mol. Struct. 1181 (2019) 338.

[26] H. Ferjani, H. Boughzala, A. Driss, J. Crystallogr. (2013) 8.

[27] Y. H. Gao, X. L. Liu, L. Sun , W. J. Le, Acta Cryst. E (2011) 1600.

[28] A. Srinivasa Rao, E. Sunil Babu, K.C. Kumara Swamy, Samar K. Das, Polyhedron 29 (2010) 1706.

[29] H. Ferjani, H. Boughzala , A. Driss, Acta Cryst. E 68 (2012) m615.

[30] R.D. Shannon, Acta Cryst A 32 (1976) 751.

[31] Z. Ouerghi, T. Roisnel, R. Fezai, R. Kefi. J. Mol. Struct. 1173 (2018) 439.

[32] C. Janiak, J. Chem. Soc. Dalton Trans. 21 (2000) 3885.

[33] A. Srinivasa Rao, U. Baruah, Samar K. Das, Inorg. Chim. Acta. 372 (2011) 206.

[34] H. Ferjani , H. Boughzala , J. Materials (2014) 8.

[35] M. Essid, Z. Aloui, M. Rzaigui, H. Marouani, J. Adv. Chem. 10 (2014) 2592.

[36] N. Elfaleh, S. Kamoun, J. Mol. Struct. 1075 (2014) 479.

[37] H. Khili, N. Chaari, M. Fliyou, S. Chaabouni, J. Adv. Chem. 8 (2014) 1566.

[38] H. Ferjani, H. Boughzal, Russ. J. Inorg. Chem. 63 (3) (2018) 349.

[39] H. Khili, N.Chaari, M. Fliyou, A. Koumina, S. Chaabouni, Polyhedron 36 (2012) 30.

[40] J. Tarasiewicz, R. Jakubas, G. Bator, J. Zaleski, J. Baran, W. Medycki, J. Mol. Struct. 932 (2009) 6.

[41] A. Kessentini, A. Ben Ahmed, T. Dammak, M. Belhouchet, Spectrochim. Acta Part A 191 (2018) 241.

[42] O. Ben Moussa, H. Chebbi, M. F. Zid, J. Mol. Struct. 1180 (2019) 72.

[43] Y. J. Wang, L. Xu, J. Mol. Struct. 875 (2008) 570.

[44] N. Leblanc, M. Allain, N. Mercier, L. Sanguinet, Cryst. Growth Des. 11 (2011) 2064.

[45] C. Hrizi, A. Samet, Y. Abid, S. Chaabouni, M. Fliyou, A. Koumina, J. Mol. Struct. 992 (2011) 96.

[46] M. Essid, Z. Aloui, V. Ferretti, S. Abid, F. Lefebvre, M. Rzaigui, C. Ben Nasr, Inorg. Chim. Acta (2017) 122.

[47] Y. Kessentini, A. Ben Ahmed, Salih S. Al-Juaid, T. Mhiri, Z. Elaoud, Opt. Mater. 53 (2016) 101.

[48] Sergey A. Adonin, Maxim N. Sokolov, Vladimir P. Fedin, Coord. Chem. Rev. 312 (2016) 1.

[49] B. V. Bukvetskii, T. V. Sedakova, A. G. Mirochnik, J. Struct. Chem. 50 (2) (2009) 322.

[50] Sergy A. Adonin , Marianna I. Rakhmanova, Denis G. Samsonenko, Maxim N. Sokolov, Vlademir P. Fedin, Inorg. Chim. Acta 450 (2016) 232.

[51] D. N. Congreve, M. C. Weidman, M. Seitz, W. Paritmongkol, N. S. Dahod, W. A. Tisdale, ACS Photonics 4 (2017) 476.

[52] E.-P. Yao, Z. Yang, L. Meng, P. Sun, S. Dong, Y. Yang, Adv. Mater. 29 (2017) 1606859.

[53] D. Yang, Y. Zou, P. Li, Q. Liu, L. Wu, H. Hu, Y. Xu, B. Sun, Q. Zhang, S.-T. Lee, Nano Energy 47 (2018) 235.

[54] B. J. Bohn, Y. Tong, M. Gramlich, M. L. Lai, M. Döblinger, K. Wang, R. L. Z. Hoye, P. Müller-Buschbaum, S. D. Stranks, A. S. Urban, L. Polavarapu, J. Feldmann, Nano Lett. 18 (2018) 5231.

[55] N. Elleuch, A. Ben Ahmed, H. Feki, Y. Abid, C. Minot, Spectrochim. Acta Part A, 121 (2014) 129.

[56] S. Guidara, H. Feki, Y. Abid, Spectrochim. Acta Part A, 115 (2013) 437.

[57] N. M. O. Boyle, A. L. Tenderholt, K. M. Langer, A Library for package-independent computational chemistry algorithms, J. Comput. Chem. 29 (2008) 839-845.

[58] A. Kessentini, T. Dammak, M. Belhouchet, J. Mol. Struct. 1149 (2017) 818.

[59] S. Soukrata, T. Dammak, T. Mhiri, M. Belhouchet, J. Cluster Science 29 (6) (2018)1051.

[60] S. Guidara, A. Ben Ahmed, Y. Abid, H. Feki, Spectrochim. Acta Part A, 127 (2014) 275.
[61] I. Abdehalim Ahmed, R. Blachnik, H. Reuter, Z. Anorg. Allg. Chem. 627 (2001) 2057.
[62] R. Jakubas, A. Piecha, A. Pietraszko, G. Bator, Phys. Rev. B 72 (2005)104107.

Figures captions

Fig.1 Molecular structure of the asymmetric unit of $[H\text{-guan}]_3[BiCl_6].H_2O$.

Fig. 2 Crystal packing of $[H\text{-guan}]_3[BiCl_6].H_2O$ compound in the (b, c) plane (hydrogen bonds shown as dashed lines).

Fig. 3 (a) and (b) Projection along the a-axis and the b-axis of the inorganic entities of the title compound.

Fig. 4 A perspective view of hydrogen bonds between acetoguanamium cations anionic clusters.

Fig. 5 A view of π–π stacking interactions between acetoguanamium cations.

Fig. 6 Superposition of the experimental (black line) and the DFT IR spectra (red line) of $[H\text{-guan}]_3[BiCl_6].H_2O$.

Fig. 7 Correlation graph of calculated and experimental frequencies.

Fig. 8 Room temperature absorption (Abs) (a) and Photoluminescence (PL) (b) spectrum of $[H\text{-guan}]_3[BiCl_6].H_2O$.

Fig. 9 Superposition of optical absorption spectra measured at room temperature (black line) and HOMO-LUMO electronic transition predicted by (TD-DFT) calculation (red line) of $[H\text{-guan}]_3[BiCl_6].H_2O$.

Fig. 10 Molecular orbital surfaces for the HOMO and LUMO of $[H\text{-guan}]_3[BiCl_6].H_2O$ compound.

Fig. 11 Density of state (DOS) spectrum of $[H\text{-guan}]_3[BiCl_6].H_2O$ compound.

Fig. 12 The Mulliken charge distribution of the $[H\text{-guan}]_3[BiCl_6].H_2O$ compound.

Fig. 13 DSC-TG curves of $[H\text{-guan}]_3[BiCl_6].H_2O$ crystal.

Tables captions

Table 1: Crystal data and structure refinement of $[H\text{-guan}]_3[BiCl_6].H_2O$.

Table 2: Bond lengths (Å) and angles (°) of the $[BiCl_6]^{3-}$ octahedron.

Table 3: Bond lengths (Å) and angles (°) of the organic cations in $[H\text{-guan}]_3[BiCl_6].H_2O$.

Table 4: Hydrogen bonds geometry of $[H\text{-guan}]_3[BiCl_6].H_2O$.

Table 5: Observed and calculated wavenumbers (cm^{-1}) of $[H\text{-guan}]_3[BiCl_6].H_2O$ with the proposed assignments.

Table 1

Empirical formula	$[H\text{-}guan]_3[BiCl_6].H_2O$
Formula Weight	818.16
Temperature (K)	293
Wavelength (Å)	0.71073
Crystal system, space group	Triclinic, P-1
Unit celle dimensions	
a (Å)	9.3143(2)
b (Å)	12.6548(4)
c (Å)	12.8962(4)
α (°)	65.723 (2)
β (°)	86.630 (2)
γ (°)	76.235 (2)
V ($Å^3$)	1344.55(7)
Z	2
Density (calculated) ($g.cm^{-3}$)	2.021
Reflections collected	27763
Independent reflections	7767
Reflections observed with $I>2\sigma(I)$	6750
R_{int}	0.103
Number of refined parameters	383
Goodness-of-fit on F^2	1.07
Final R indices [$I>2\sigma(I)$]	$R_1 = 0.048$ and $wR_2 = 0.122$
Largest diff. peak and hole, e $Å^{-3}$	2.07 and -3.22
CCDC N°	1907441

Table 2

$[BiCl_6]^{3-}$ anion			
Bi1—Cl4	2.5709 (15)	Cl4—Bi1—Cl3	95.75 (6)
Bi1—Cl3	2.6538 (17)	Cl4—Bi1—Cl1	89.19 (5)
Bi1—Cl1	2.7129 (15)	Cl3—Bi1—Cl1	87.55 (5)
Bi1—Cl2	2.7215 (14)	Cl4—Bi1—Cl2	89.18 (5)
Bi1—Cl6	2.7409 (18)	Cl3—Bi1—Cl2	86.65 (5)
Bi1—Cl5	2.8602 (15)	Cl1—Bi1—Cl2	173.79 (5)
		Cl4—Bi1—Cl6	86.43 (6)
		Cl3—Bi1—Cl6	176.06 (5)
		Cl1—Bi1—Cl6	95.78 (6)
		Cl2—Bi1—Cl6	90.10 (6)
		Cl4—Bi1—Cl5	175.37 (6)
		Cl3—Bi1—Cl5	88.82 (6)
		Cl1—Bi1—Cl5	91.72 (5)
		Cl2—Bi1—Cl5	90.38 (5)
		Cl6—Bi1—Cl5	88.97 (6)

Table 3

$C_4H_8N_5$ cations			
Distances (Å)			
N1—C1	1.328 (7)	C2—C4	1.484 (8)
N1—C3	1.344 (7)	C6—C8	1.481 (9)
N2—C2	1.359 (7)	C10—C12	1.453 (8)
N2—C1	1.366 (7)	N9—C5	1.323 (7)
N3—C2	1.302 (7)	N10—C7	1.316 (7)
N3—C3	1.370 (7)	N11—C11	1.331 (7)
N4—C1	1.307 (7)	N11—C9	1.337 (8)
N5—C3	1.324 (7)	N12—C10	1.308 (6)
N6—C5	1.324 (7)	N12—C9	1.364 (7)
N6—C7	1.347 (6)	N13—C10	1.357 (7)
N7—C6	1.357 (7)	N13—C11	1.357 (7)
N7—C5	1.361 (8)	N14—C11	1.320 (8)
N8—C6	1.312 (7)	N15—C9	1.328 (7)
N8—C7	1.375 (7)		
Angles (°)			
C2—N2—C1	120.2 (5)	N9—C5—N6	120.3 (6)
C2—N3—C3	116.3 (4)	N9—C5—N7	118.0 (5)
C1—N1—C3	116.0 (5)	N6—C5—N7	121.6 (5)
N8—C6—N7	121.4 (5)	C11—N11—C9	115.9 (5)
N8—C6—C8	121.6 (5)	C10—N12—C9	116.0 (5)
N7—C6—C8	117.0 (5)	C10—N13—C11	120.1 (4)
N10—C7—N6	118.5 (5)	N4—C1—N1	121.7 (5)
N10—C7—N8	116.0 (5)	N4—C1—N2	117.6 (5)
N6—C7—N8	125.5 (5)	N1—C1—N2	120.6 (5)
N2—C2—C4	117.1 (5)	N3—C2—N2	121.3 (5)
N5—C3—N1	119.2 (5)	N3—C2—C4	121.6 (5)
N5—C3—N3	115.4 (5)	N15—C9—N11	117.8 (5)
N1—C3—N3	125.5 (5)	N15—C9—N12	116.4 (6)
C5—N6—C7	115.6 (5)	N11—C9—N12	125.8 (5)
C6—N7—C5	119.9 (5)	N12—C10—N13	121.3 (5)
C6—N8—C7	115.9 (5)	N12—C10—C12	121.0 (5)
N14—C11—N11	120.2 (5)	N13—C10—C12	117.7 (5)
N14—C11—N13	118.9 (5)	N11—C11—N13	120.9 (5)

Table 4

D—H···*A*	*D*—H	H···*A*	*D*···*A*	*D*—H···*A*
N4—H4A···N12^{i}	0.90 (9)	2.09 (9)	2.973 (8)	169 (7)
N4—H4B···Cl3	0.84 (9)	2.68 (9)	3.393 (6)	144 (8)
N5—H5A···Cl6^{ii}	0.89 (2)	2.48 (4)	3.299 (5)	153 (7)
N5—H5B···N8^{iii}	0.89 (2)	2.29 (3)	3.161 (7)	167 (8)
N2—H2···Cl5	0.87 (2)	2.42 (5)	3.202 (5)	150 (9)
N7—H7···O1W	0.87 (2)	1.79 (2)	2.660 (7)	177 (8)
N9—H9A···N6^{i}	0.88 (2)	2.22 (2)	3.103 (8)	173 (7)
N9—H9B···Cl1	0.88 (2)	2.43 (6)	3.176 (5)	142 (7)
N10—H10A···Cl1^{i}	0.88 (2)	2.44 (3)	3.296 (5)	163 (7)
N10—H10B···N3^{iii}	0.871 (19)	2.13 (2)	2.998 (7)	173 (5)
N13—H13···Cl2^{iv}	0.87 (2)	2.29 (3)	3.137 (4)	163 (8)
N14—H14A···Cl5^{v}	0.876 (19)	2.54 (3)	3.394 (6)	164 (5)
N14—H14B···Cl2^{iv}	0.87 (2)	2.74 (4)	3.553 (6)	156 (7)
N15—H15A···N1^{i}	0.88 (2)	2.44 (3)	3.312 (8)	168 (8)
N15—H15B···Cl4^{vi}	0.88 (2)	2.57 (3)	3.425 (6)	163 (6)
O1W—H1W1···Cl6^{vi}	0.87 (2)	2.47 (4)	3.291 (7)	158 (8)
O1W—H2W1···Cl5	0.86 (2)	2.47 (5)	3.295 (7)	161 (10)

The ring-interactions with Cg–Cg distances (Å)	
C_{g1}-C_{g2}	3.928(6)
C_{g2}-C_{g3}	4.028(5)
C_{g3}-$C_{g3}^{(vii)}$	3.684(5)

Symmetry codes: (i) −*x*+2, −*y*, −*z*+1; (ii) *x*, *y*−1, *z*; (iii) −*x*+1, −*y*, −*z*+1; (iv) *x*−1, *y*, *z*−1; (v) −*x*+1, −*y*+1, −*z*+1; (vi) −*x*+2, −*y*+1, −*z*+1, (vii) -1-x, -1-y, -z.

C_{g1}, C_{g2} and C_{g3} are the centroid of H-guan (1), H-guan (2) and H-guan (3) respectively.

Table 5

FT-IR		Assignment
Experimental	Calculated	
-	3784 w	ν_{as}(O-H)
-	3689 w	ν_{as}(O-H)
-	3623 w	ν_{s}(O-H)
3520 vw	3571 w	ν_{s}(O-H)
-	3428 w	$\nu_{as}(NH_2)$
-	3376 m	$\nu_{as}(NH_2)$
3303 m	3301 m	$\nu_{s}(NH_2)$
-	3260 m	$\nu_{s}(NH_2)$
3217 m	-	ν(N-H)
3169 m	-	ν(N-H)
	3092 m	ν(N-H)
3059 m	-	$\nu_{as}(CH_3)$
2925 m - 2852 m	-	$\nu_{s}(CH_3)$
2621 w	2435 vs	Combination bands and overtones
-	1758 w - 1716 m	$\delta(H_2O)$
1670 vs	1690 s	$\delta_{as}(NH_2)$
1624 vs	1640 s	$\delta_{s}(NH_2)$
1525 s	1570 w	ω (NH_2)
1502 s	1519 w	δ_{as}(CH3)
1490 s	1492 m	δ_{s}(CH3)
1459 s	1449 m	δ_{s}(CH3) + ν (C=N)
1418 s	-	δ_{s}(CH3) + ω (NH_2)
1360 s	1387 w	δ_{s}(CH3) + t(NH_2)
1338 m	1322 vw	ρ (NH_2)
1269 m	1290 vw	ω (CH_3)
1174 m	1180 vw	t(NH_2)
1089 m	1094 vw	ν_{as}(C-N-C)
1042 w	1088 vw	ω(CH_3)
1027 w	-	ρ (NH_2)
1011 w	-	ρ (CH_3)
1000 w	1000 w	N-H in plane bending
971 m	955 w	N-H out of plane bending
-	874 m	ν_{s} (C-N-C)
786 s	812 m	ρ (H_2O)
702 m	722 w	
627 m	623 vw	δ(C-N-C)
556 vs	580 vw	δ(C-C-N)- δ (N-C-N)
-	219 w	ν_{as}(Bi-Cl)
-	166 w	ν_{s}(Bi-Cl)

Abbreviations: **s**: strong, **w**: weak, **v**: very, **m**: medium, **ν**: stretching; ***δ***: out of plane bending; **ρ** : rocking , **t**: twisting, **ω**: wagging.

* A new hybrid material $[C_4H_8N_5]_3BiCl_6H_2O$ was synthesized.
* HOMO-LUMO energy gap explains the charge transfer interactions in the molecule.
* UV spectrum was interpreted and attributed based en TD-DFT calculation.

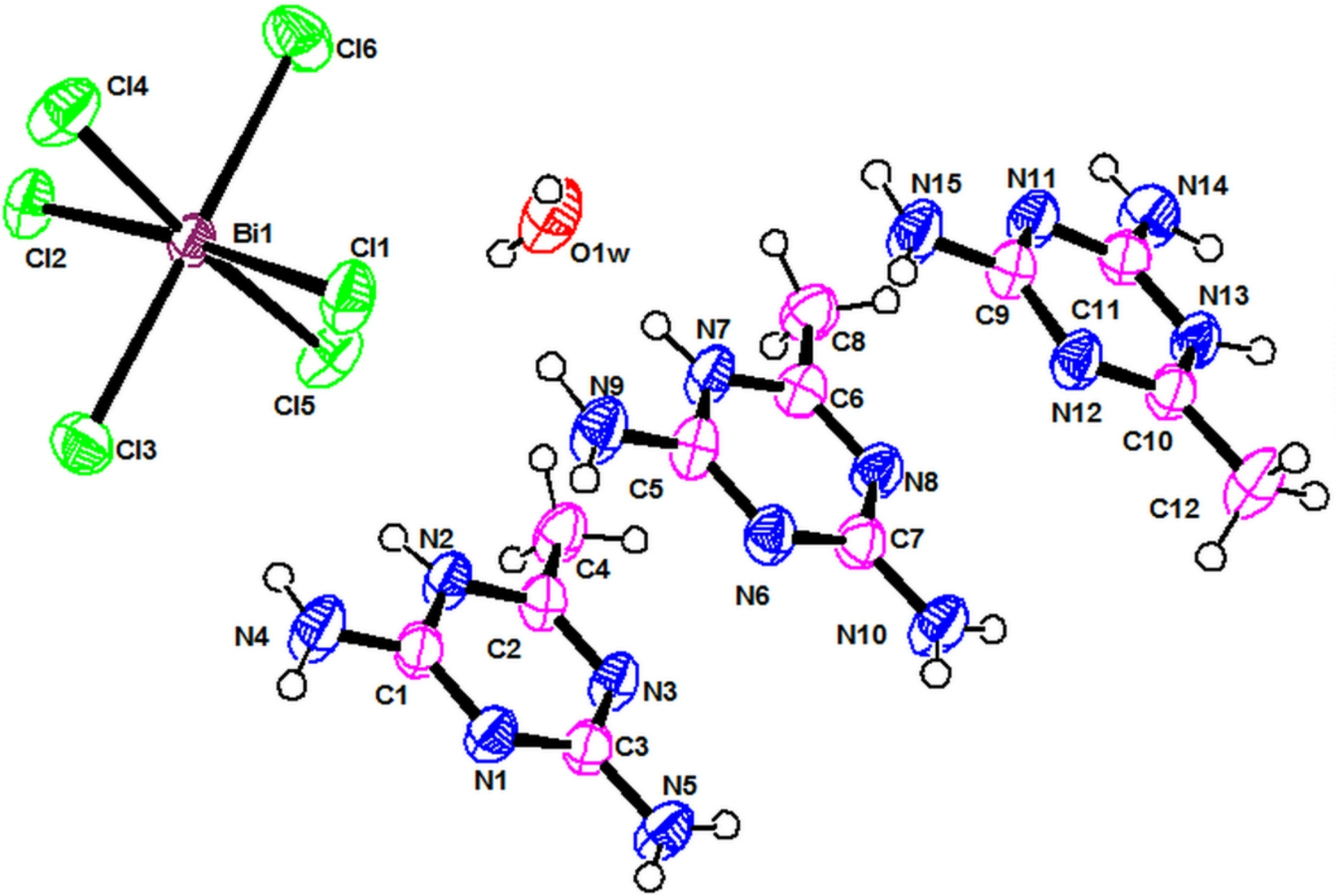
Cl6
Cl4
Cl2
Bi1
Cl1
Cl5
Cl3
O1w
N15
N11
N14
N7
C8
C9
C11
N13
N9
C6
N12
C10
C5
N8
C12
N2
C4
C7
N6
N4
C2
N10
C1
N3
C3
N1
N5

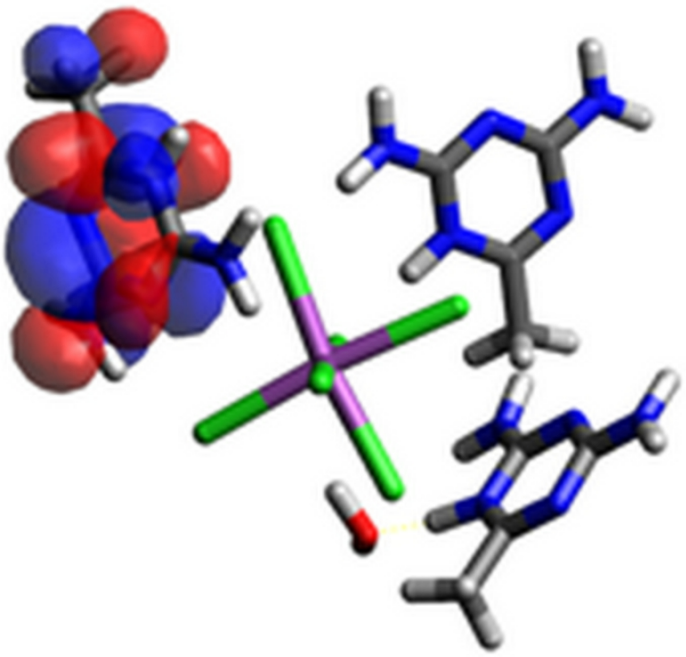

LUMO PLOT

(Excited State)

E_{LUMO} = -1.95 *eV*

$\Delta E_{HOMO-LUMO}$ = 3.71 *eV*

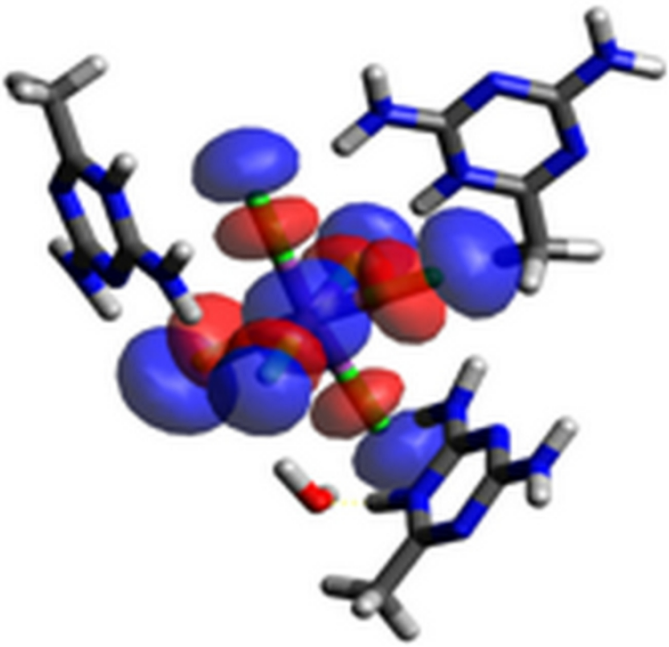

E_{HOMO} = -5.66 *eV*

HOMO PLOT

(Ground State)

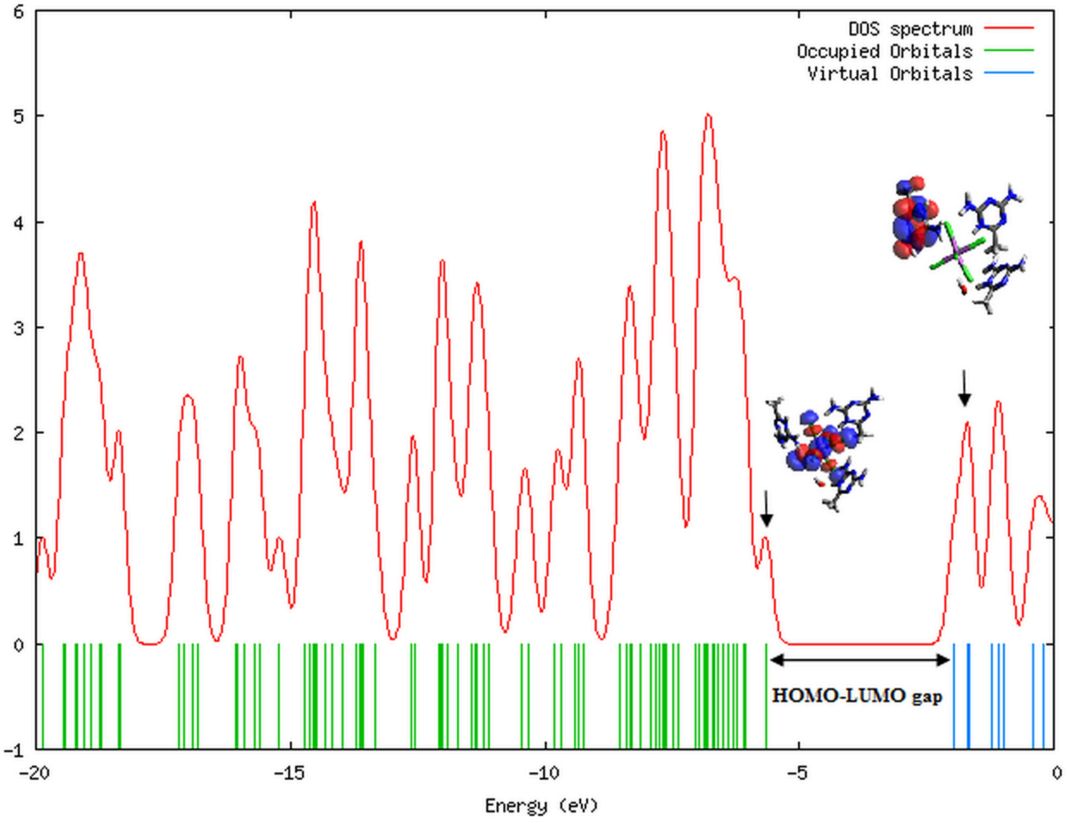
DOS spectrum
Occupied Orbitals
Virtual Orbitals
HOMO-LUMO gap
Energy (eV)
6
5
4
3
2
1
0
-1
-20
-15
-10
-5
0

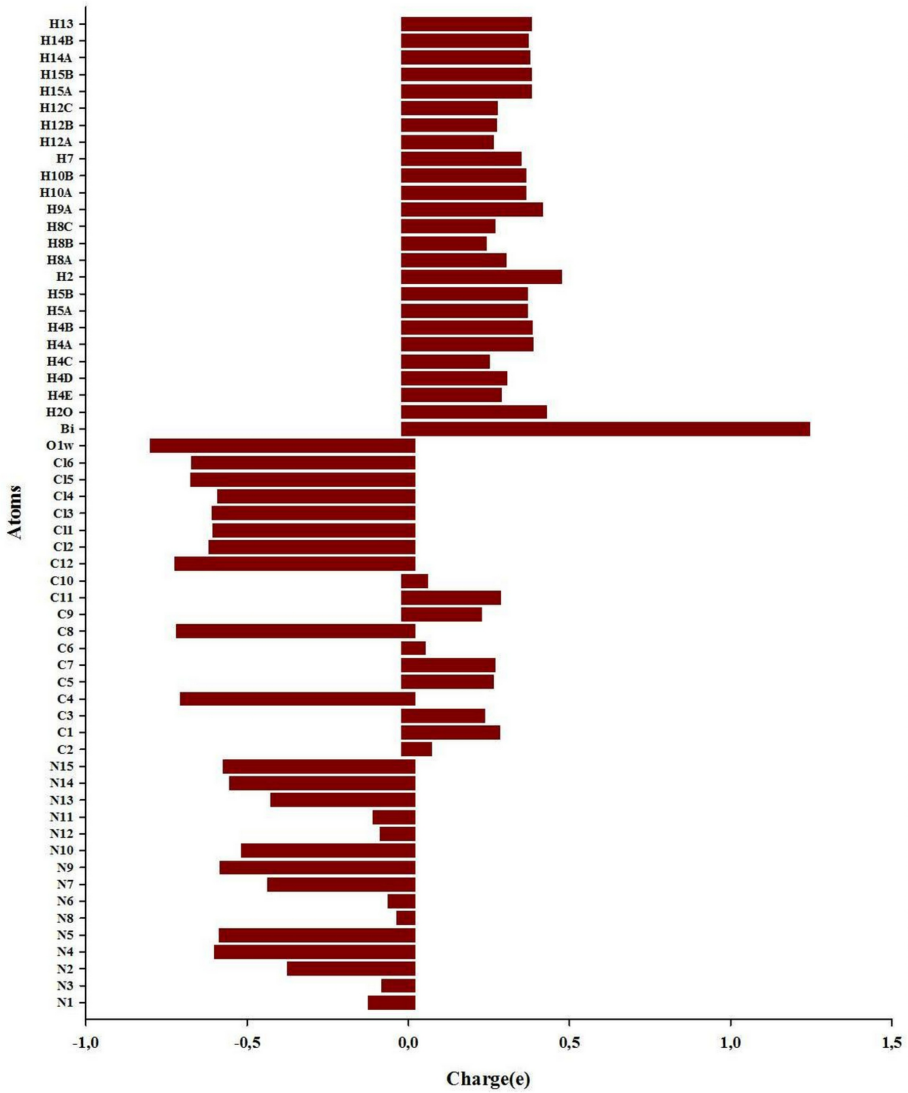
H13
H14B
H14A
H15B
H15A
H12C
H12B
H12A
H7
H10B
H10A
H9A
H8C
H8B
H8A
H2
H5B
H5A
H4B
H4A
H4C
H4D
H4E
H2O
Bi
O1w
Cl6
Cl5
Cl4
Cl3
Cl1
Cl2
C12
C10
C11
C9
C8
C6
C7
C5
C4
C3
C1
C2
N15
N14
N13
N11
N12
N10
N9
N7
N6
N8
N5
N4
N2
N3
N1
Atoms
-1,0
-0,5
0,0
0,5
1,0
1,5
Charge(e)

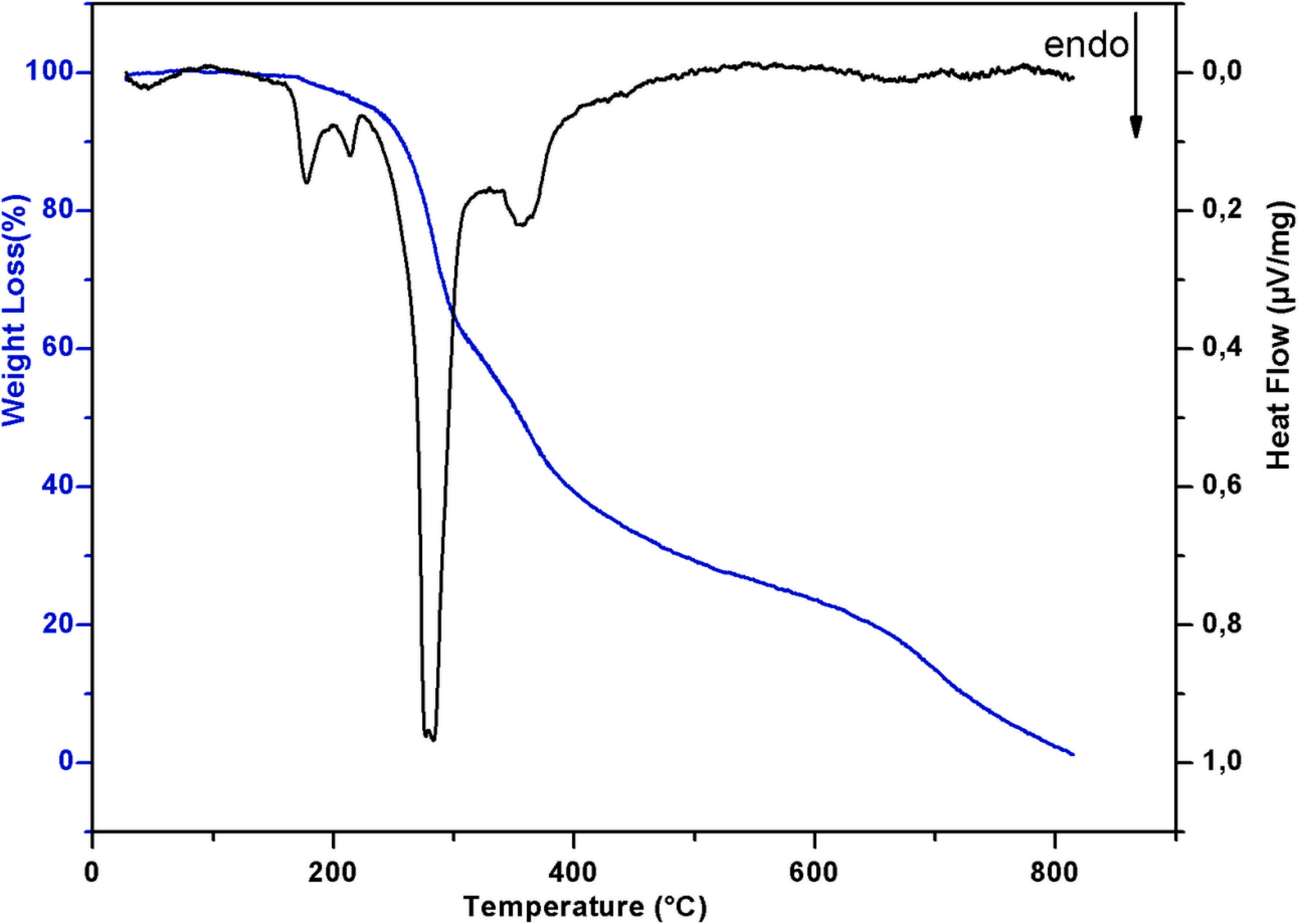
endo
Weight Loss(%)
Heat Flow (µV/mg)
Temperature (°C)
100
80
60
40
20
0
0,0
0,2
0,4
0,6
0,8
1,0
0
200
400
600
800

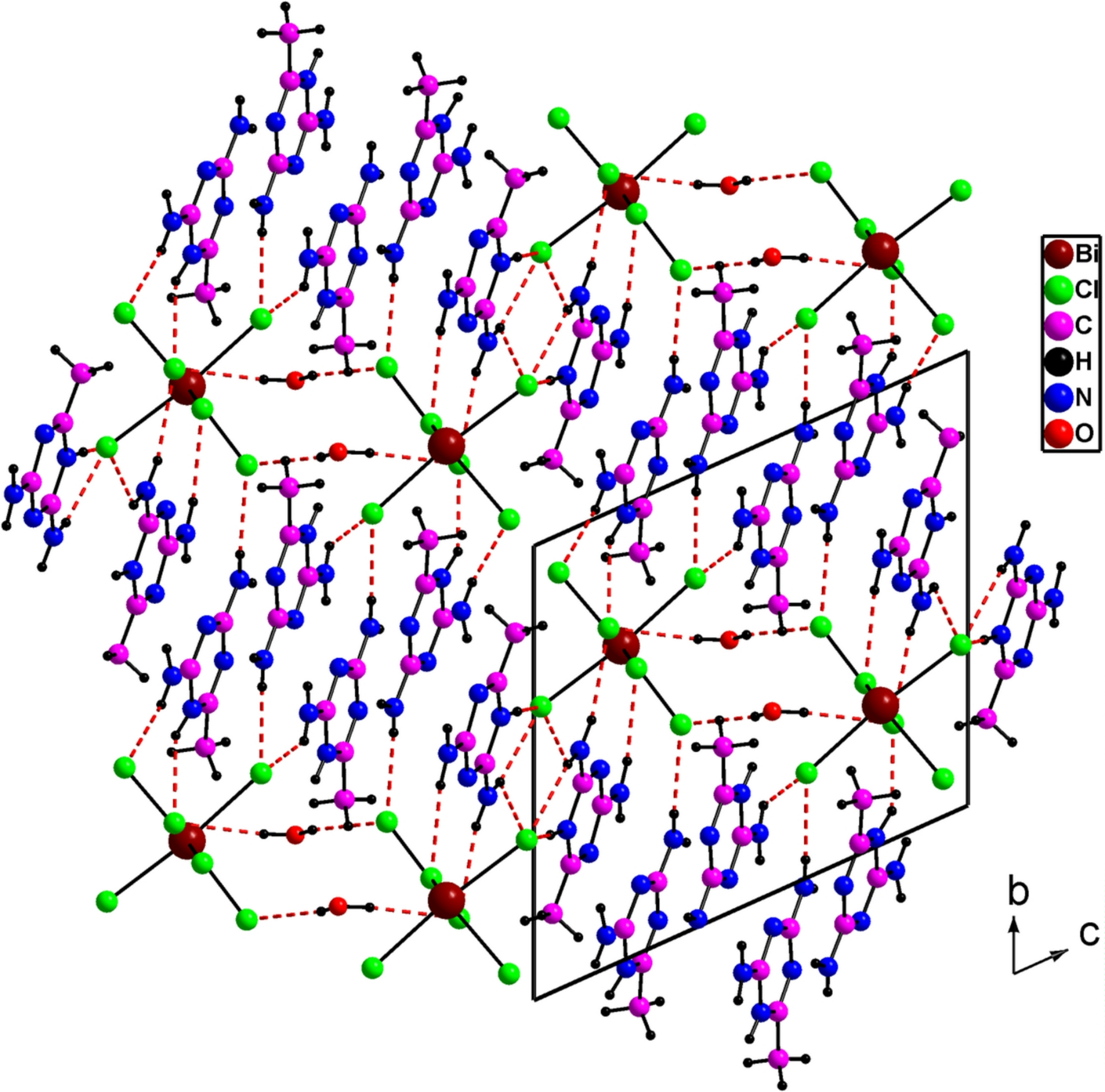
Bi
Cl
C
H
N
O
b
c

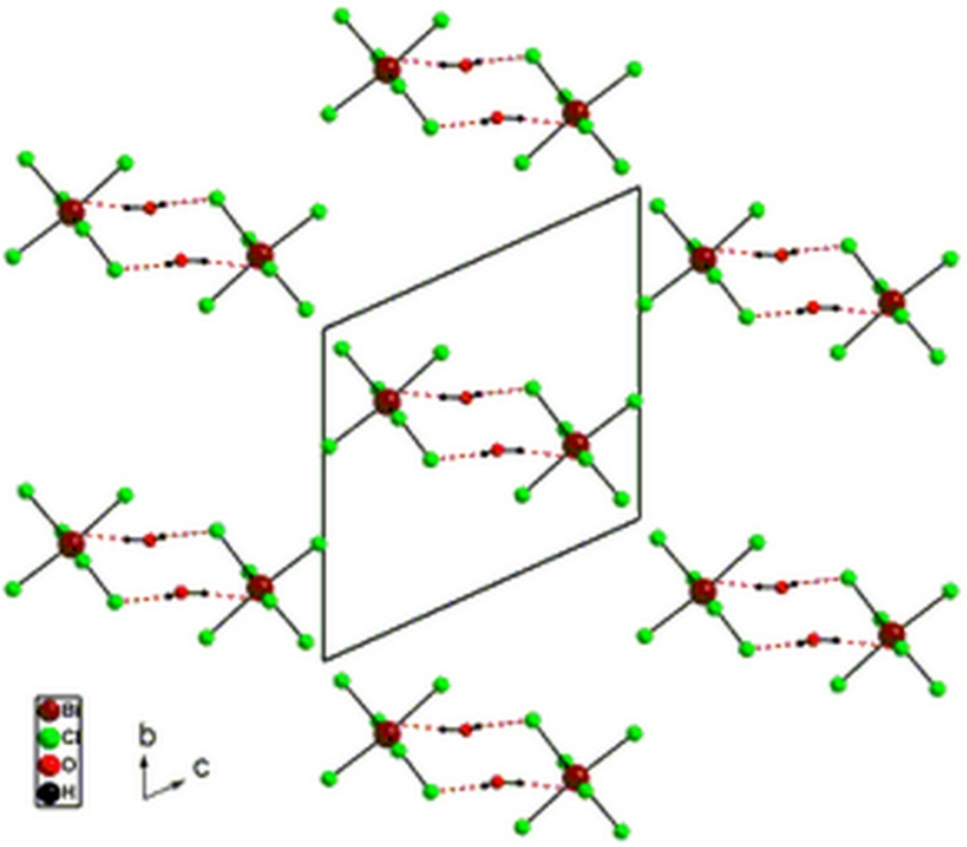

(a)

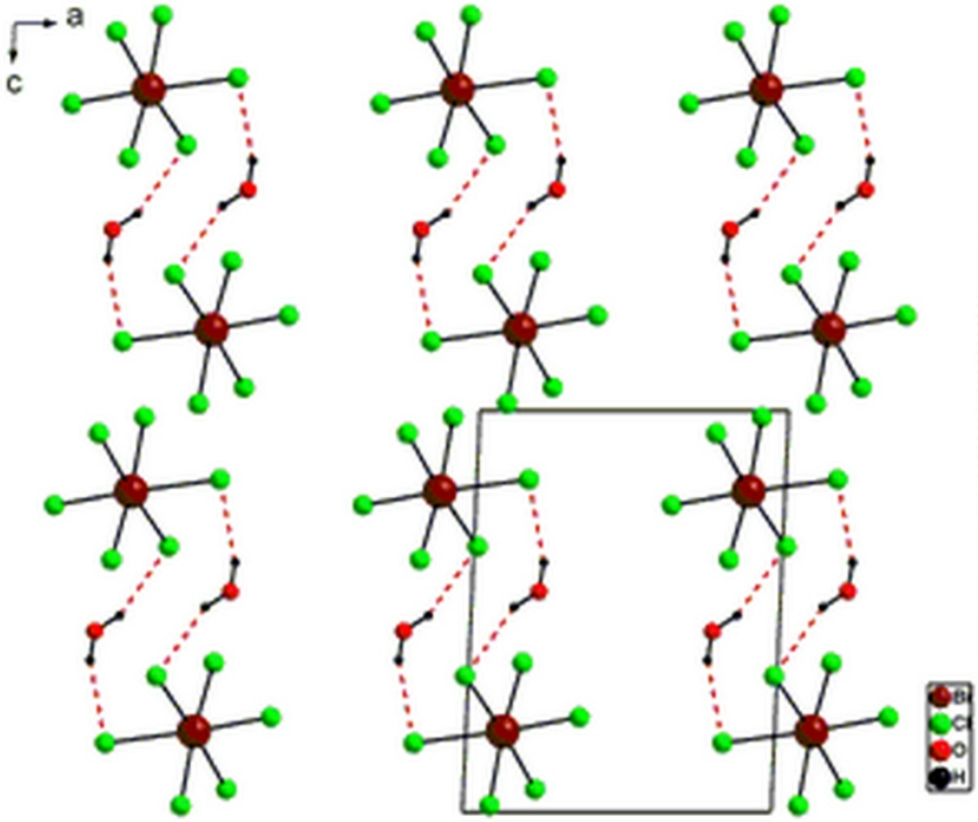

(b)

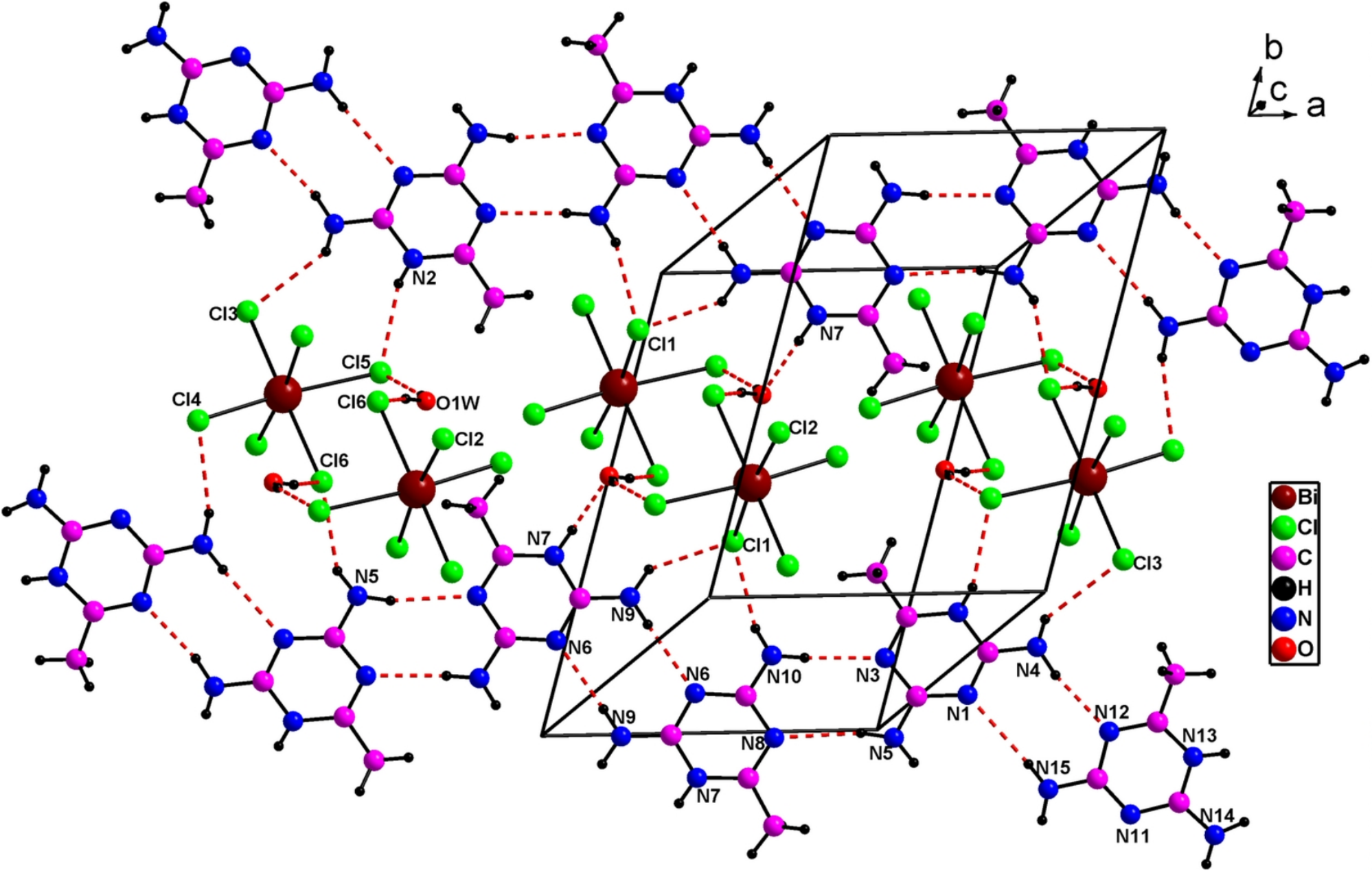
b
c
a
Bi
Cl
C
H
N
O
Cl3
N2
Cl5
Cl4
Cl6
O1W
Cl2
Cl6
N7
Cl1
Cl2
N7
Cl1
Cl3
N5
N9
N6
N6
N10
N3
N4
N9
N1
N12
N13
N8
N5
N15
N7
N14
N11

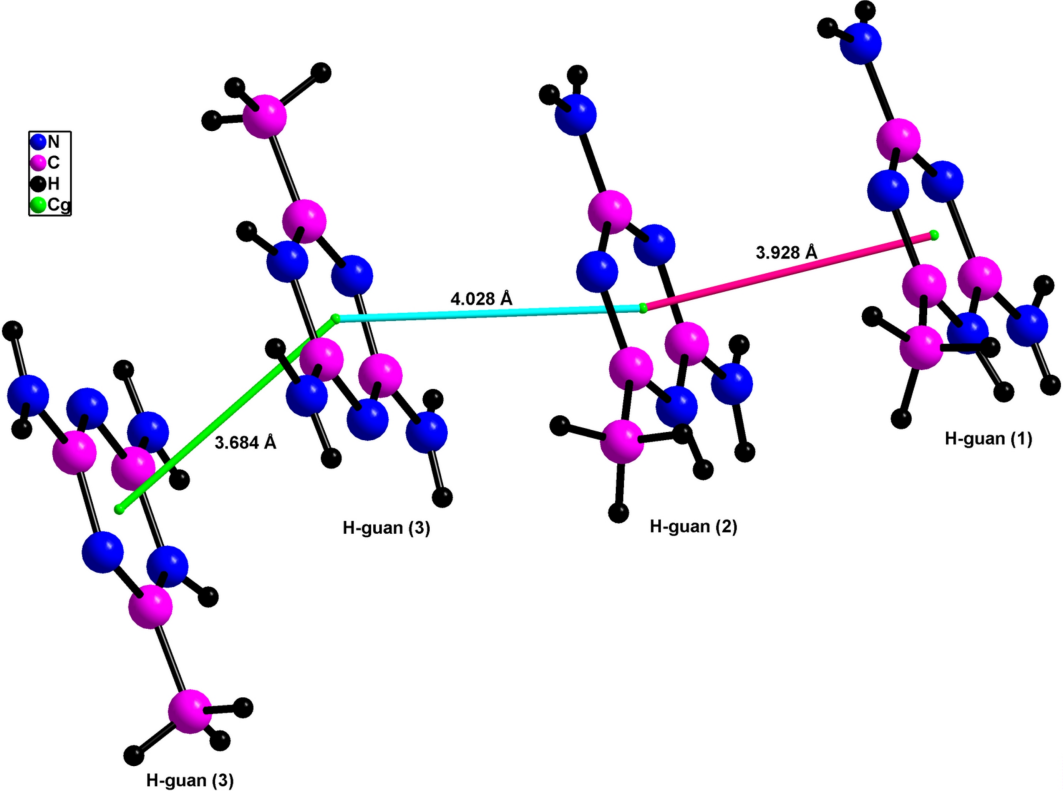
N
C
H
Cg
3.684 Å
4.028 Å
3.928 Å
H-guan (3)
H-guan (2)
H-guan (1)
H-guan (3)

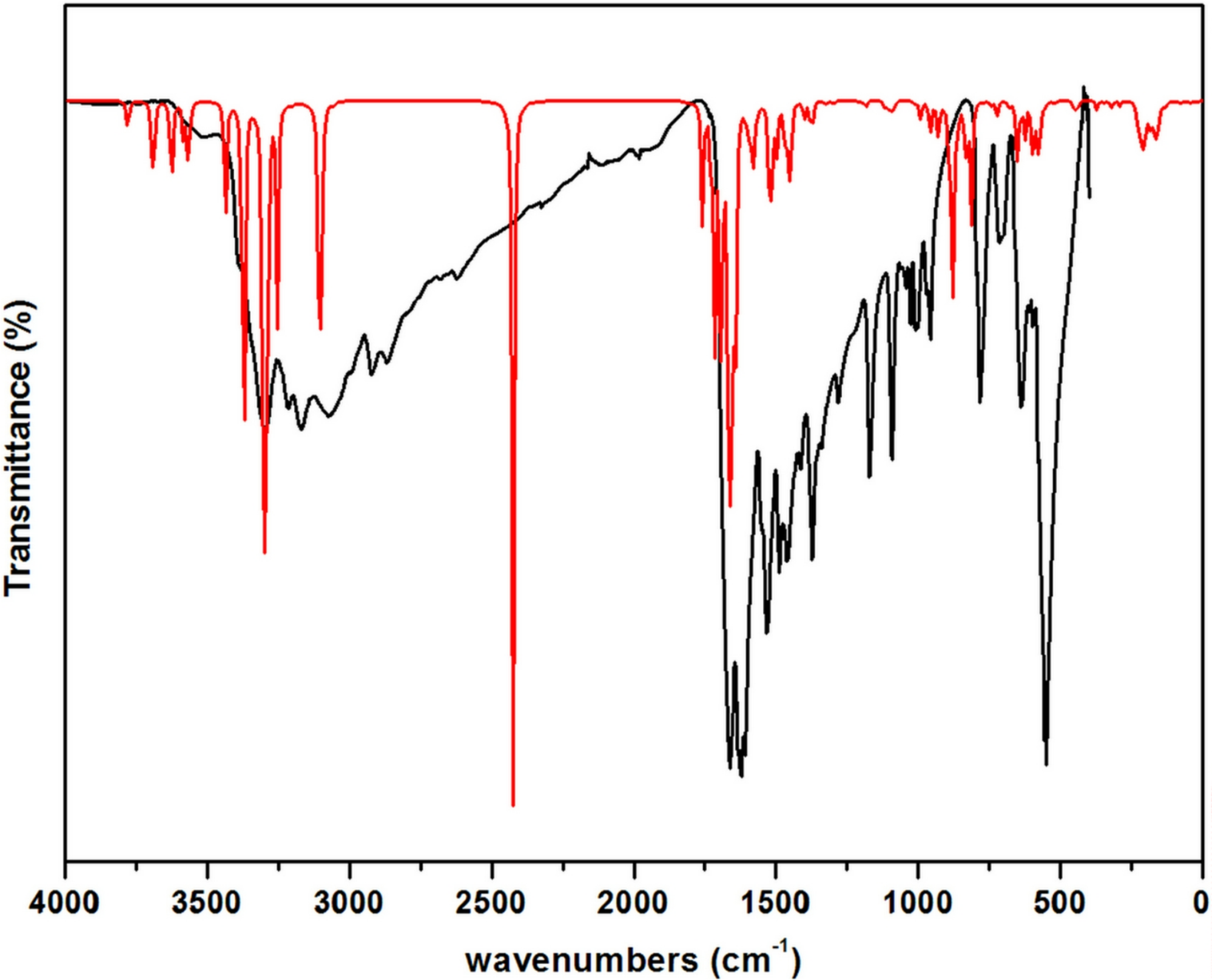
Transmittance (%)
4000
3500
3000
2500
2000
1500
1000
500
0
wavenumbers (cm-1)

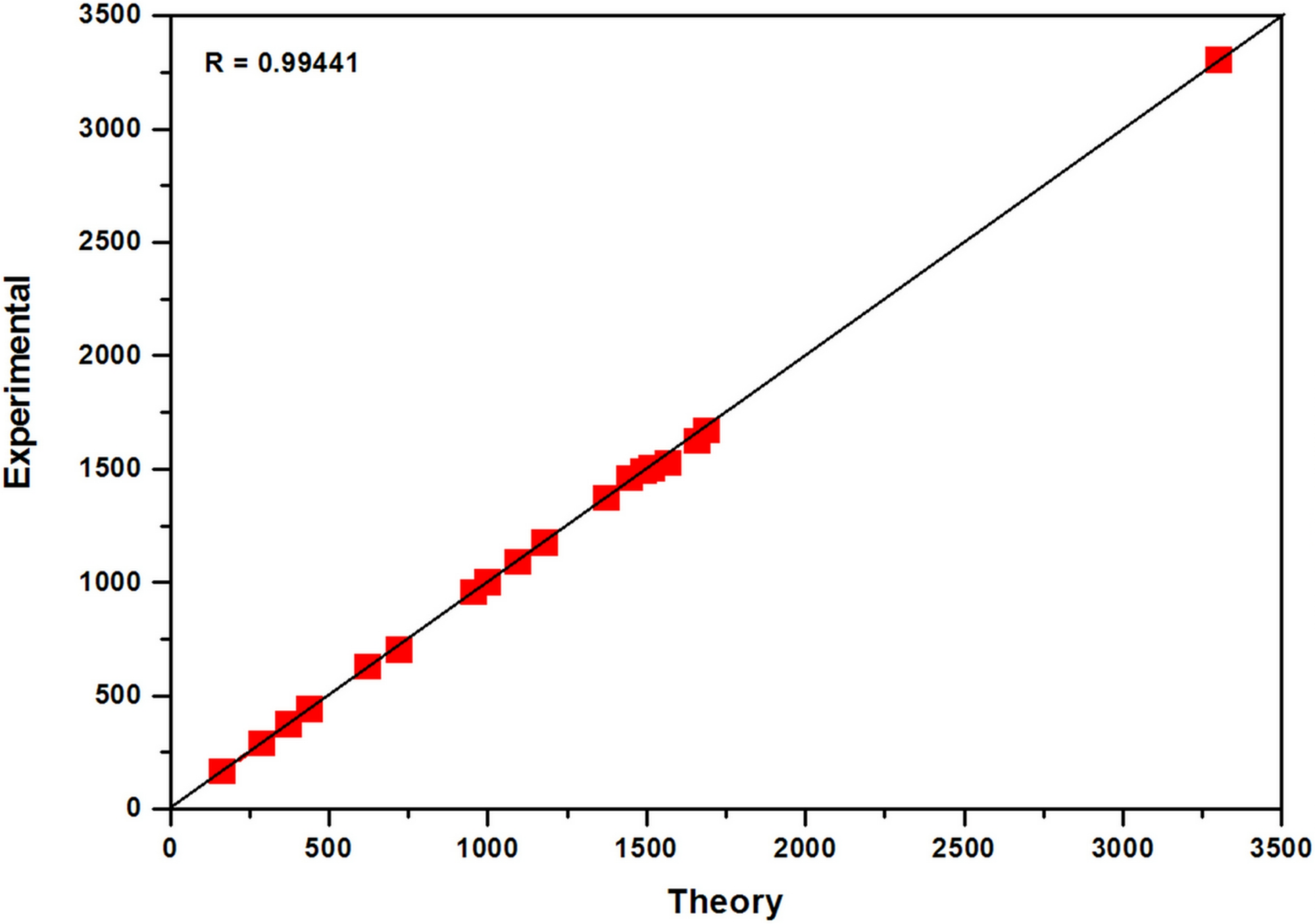
R = 0.99441
Experimental
Theory
0
500
1000
1500
2000
2500
3000
3500

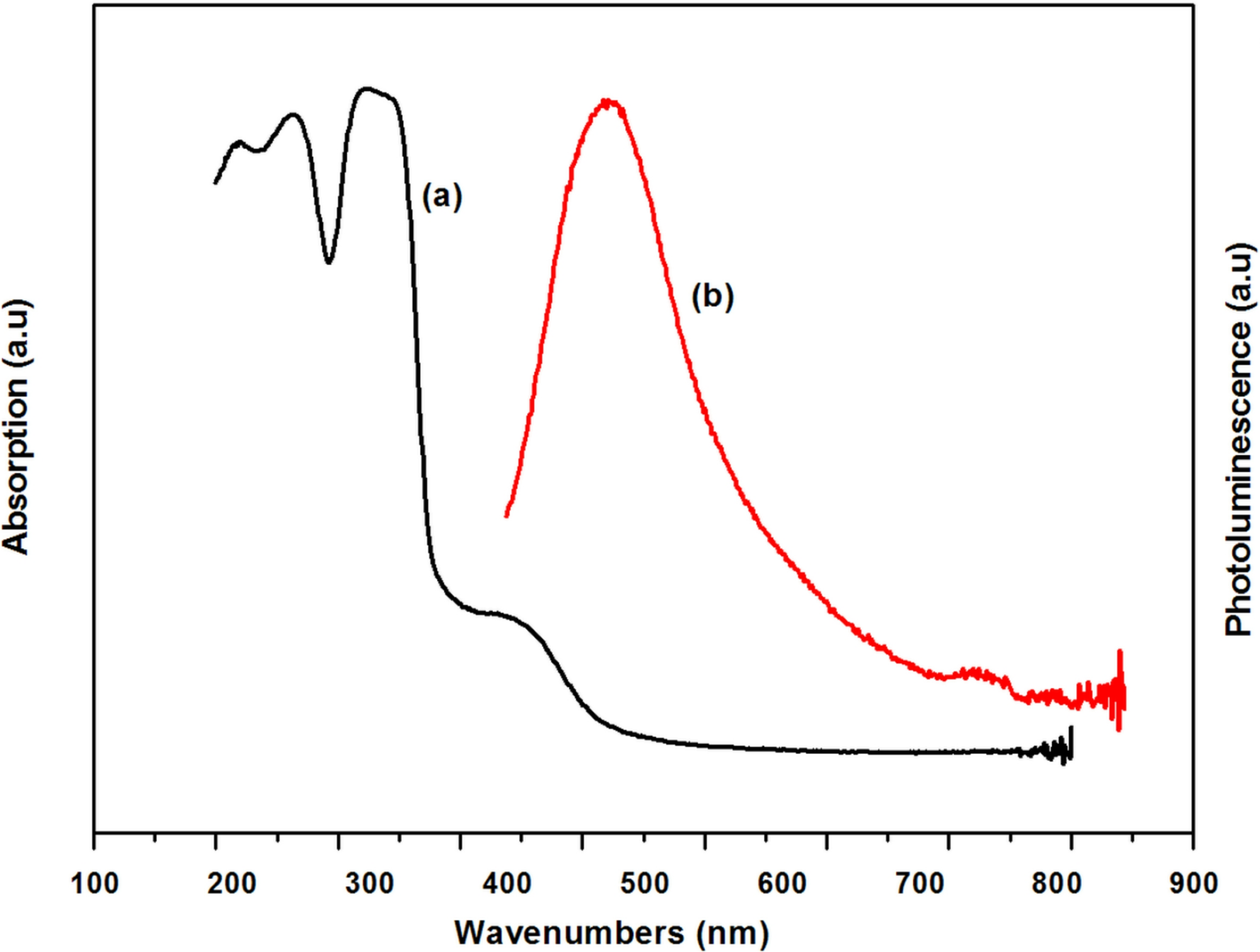
(a)
(b)
Absorption (a.u)
Photoluminescence (a.u)
100
200
300
400
500
600
700
800
900
Wavenumbers (nm)

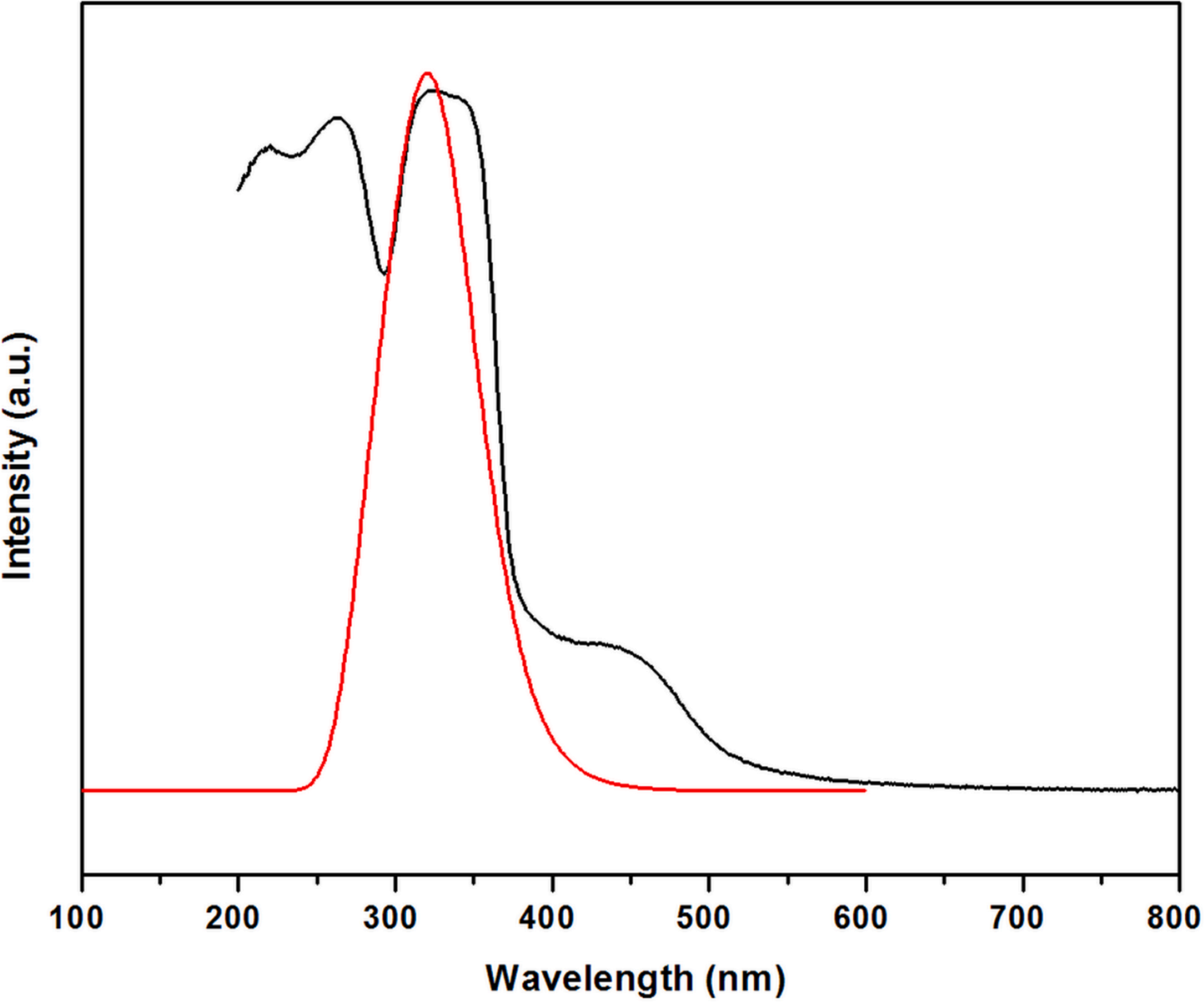
Intensity (a.u.)
100
200
300
400
500
600
700
800
Wavelength (nm)

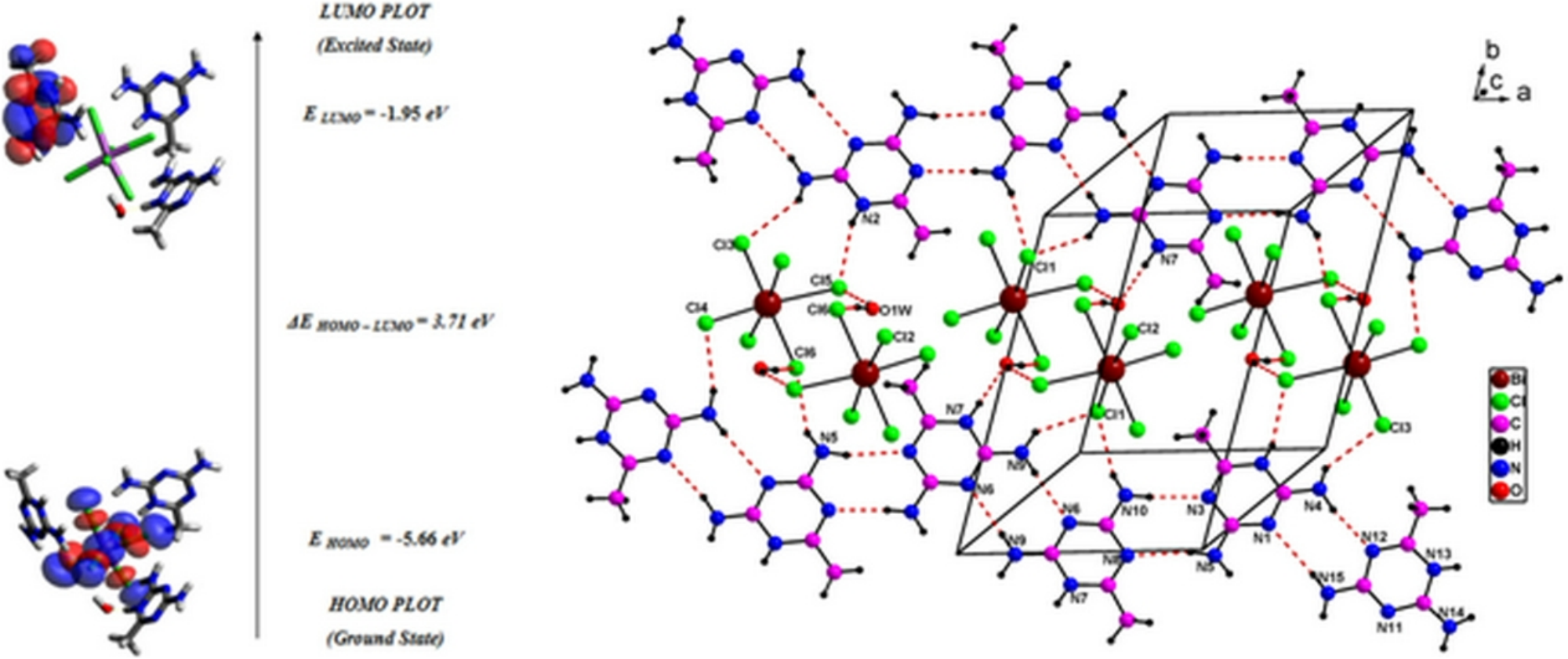
LUMO PLOT
(Excited State)
E LUMO = -1.95 eV
ΔE HOMO - LUMO = 3.71 eV
E HOMO = -5.66 eV
HOMO PLOT
(Ground State)
b
c
a
Cl3
Cl5
Cl4
Cl6
O1W
Cl2
Cl1
N2
N7
N5
N6
N10
N3
N4
N1
N9
N8
N12
N13
N15
N14
N11
Cl
C
H
N
O